

RAPID BRIGHTNESS VARIATIONS AS A TOOL TO ENHANCE SATELLITE DETECTABILITY

Myrtille Laas-Bourez⁽¹⁾, Alain Klotz^(2,1), Etienne Ducrotte⁽³⁾, Michel Boër⁽¹⁾, Gwendoline Blanchet⁽³⁾,

⁽¹⁾ *Observatoire de Haute Provence (CNRS), 04870 Saint Michel l'Observatoire, France,
Email: Myrtille.Laas@oamp.fr, Michel.Boer@oamp.fr*

⁽²⁾ *Centre d'Etude Spatiale des Rayonnements (UPS-CNRS), 9 av. du Colonel Roche, 31028 Toulouse, France
Email: alain.klotz@cesr.fr*

⁽³⁾ *Centre National d'Etudes Spatiales, 18 av. Edouard Belin, 31401 Toulouse, France
Email: etienne.ducrotte@cnes.fr, gwendoline.blanchet@cnes.fr*

ABSTRACT

To preserve the space environment for future generations and ensure the safety of space missions, we have to improve our knowledge of the debris at all altitudes. Since 2004, we have started to observe and study satellites and debris on the geostationary orbit. We use a network of robotic telescopes called TAROT (Télescopes Action Rapide pour les Objets Transitoires - Rapid Action Telescope for Transient Objects) which are located in France and Chile. This system processes the data in real time. Its wide field of view is useful for detection, systematic survey and to follow both catalogued and uncatalogued objects. The TAROTs are 25 cm telescopes with a wide field of view of 1.86deg x 1.86deg. It can detect objects up to 17th magnitude with an integration time of 30 seconds, corresponding to an object of 50cm in the geostationary belt with a 0.2 albedo. Tiny debris are also dangerous for space mission and satellites. To detect them, we need either to increase the TAROT sensitivity or to observe them in optimal light conditions.

Last year we detected very important magnitude variations from several geostationary satellites during observations close to equinoxes. The brightness of a geostationary satellite evolves during the night and during the year, depending on the angle between the observer, the satellite and the sun. Geostationary satellites will be brighter near March 1st and of October 10th, at their exit of the shade. In this period the sun crosses the equatorial plan of the Earth, the enlightened surface will reach a maximum during a limited periods of time (about 30 minutes), provoking a short, bright flash. This phenomenon is used in two ways: first, it allows to detect smaller objects, which are usually below the detection limit, enhancing the sensitivity of the survey. Secondly, for longer objects the light curve during and outside the flash contains information on the object intrinsic geometry and reflectivity.

In this paper we discuss how the various surfaces of satellites, the reflection laws and the geometric lighting

conditions can produce a flash. Then we present the results obtained with simulations and compare them with TAROT observations during two campaigns.

1. INTRODUCTION

Geostationary orbit is a valuable operational resource unfortunately polluted by debris [1]. Hence, precise knowledge of the geostationary population is necessary to preserve space missions and environment, especially to avoid debris impacts. Ground based telescopes are well suited for observing space objects, particularly in the vicinity of the geostationary belt, but still limited by their sensitivity.

TAROT (<http://tarot.obs-hp.fr/>) is a system of two completely autonomous and fully automated 25cm telescopes. The first one is installed at OCA (Calern Observatory in France) and the second one at ESO La Silla, Chile [2].

Both instruments have for primary goal the search for the prompt optical counterpart of Gamma-Ray Bursts (GRB) [3],[4]. When there is no GRB, they are used for astronomical research in various fields [5] and for the purpose presented here.

To focus on technical aspects, the field of view is: 1.86deg x 1.86deg. This optical system can detect an astronomical object of 17th magnitude within an integration time of 30 seconds, corresponding to an object of 50cm in the geostationary belt with a 0.2 albedo. For comparison, the GALAXY 2 satellite is 12.21 corrected magnitude for 10 second duration of exposure [6].

In spite of their agility and swiftness that allow observations of the Low Earth Orbit (LEO), TAROT telescopes can't detect small GEO (Geostationary Earth Orbit) or GTO (Geostationary Transfer Orbit) objects.

The satellite observation is possible if the satellite is above the horizon of the observer and lighted by the

Sun. For distant orbits or small objects it is necessary that the Sun is under the horizon. Satellites in geostationary orbits are fixed for a given observer, thus a telescope will observe only a part of the geostationary belt. The observable objects are of several types: operational satellites, decommissioned satellites, debris, and fragment (painting, ergol), launchers (in GTO).

The visual magnitude of a geostationary satellite evolves during the night and the year, because it depends on the angle between the observer, the satellite and the sun. There are two periods of eclipse for geostationary objects (42 days in Mars - April and 42 days in September - October), during which objects are not visible any more during approximately one hour. The geostationary satellites will reach their maximum in brightness when they are on the shade of the Earth. For Calern observatory {GPS 6.9238° E 43.7522° N 1270} this phenomenon is visible near March 1st and of October 10th. In this period the sun crosses the equatorial plan of the Earth, the lighted surface of an object can be maximal for a limited periods of time (about 30 minutes), provoking a short, bright flash.

Here, we propose to use this phenomenon may be used in two ways: first, it allows to detect smaller objects, which are usually below the detection limit, enhancing the sensitivity of the survey. Second, for larger objects, the light curve during and outside the flash contains information on its intrinsic geometry and reflectivity.

In this paper we discuss how the various satellite surfaces, the reflection laws and the geometric conditions can produce a flash.

Then we present the results obtained with simulations and compare them with the TAROT data acquired during two observation campaigns.

2. SATELLITE SURFACES AND GEOMETRIC LIGHTING CONDITIONS

2.1. The Reflecting Surfaces of Satellites

Communications satellites consist generally of a bus, solar panels and large white antennas.

Communication antennas are designed to optimize the coverage area according to the demands of the final customer. For the geostationary satellites they are white, with a diameter lower than 2.3 m except particular cases that makes a surface on the order of 4 m². The order of spans surface is 40 m². The size minimum of solar panels is of the order of 30 m² for satellites of type 3-axes, although there are satellites 3-axes such as AMC-12 who size of the panels is more than 100 m².

A satellite can be analysed into five surfaces of reflection or light-scattering [7]:

- The solar spans have a rate of absorption range from 0.7 to 0.92, depending on the technology used. For the visible wavelengths, the diffuse reflection of the solar radiation is weak.

- White antennas are parabolic and could be approximated by surfaces of specular reflection. Some can be protected with a reflective plane surfaces in radome.

- Parts of the body are isolated with MLI (Multi Layer Insulator). This material reflects approximately 80 % (and up to 99%) of the solar radiation.

- White paints PSB are used on external surfaces. This type of cover absorbs on average 20 % of the solar radiation for the PSB.

- Optical solar reflectors (OSRs) are conceived to reflect a maximum of the solar radiation, approximately 90 %.

The characteristics of the objects which were observed from TAROT Calern are summarized in Tab. 1.

Table 1: Satellites observed with TAROT Calern

Name	Version	Position (degrees)	Body dimensions (m)	Total wing-span (m)	White antennas	Direction of antenna
Syracuse 3A	Spacebus 4000 B3	+47°E	2.3 x 1.8 x 3.7	30	1 big	France
Syracuse 3B	Spacebus 4000 B3	-5.2°E	2.3 x 1.8 x 3.7	30	1 big	Pacific ocean
Atlantic bird 3	Spacebus 3000 B3	-5.2°E	2.3 x 1.8 x 3.7	30	2 big	France
Hispasat 1C/1D	Spacebus 3000 B2	-30°E	2.3 x 1.8 x 2.8	≈28	3	Spain/Europe
Spainsat	FS 1300	-30°E	5.4 x 2.8 x 2.2	31,4	many small	Spain

To valid our first simulations we modelled satellites as three different surfaces (see Fig. 1): the body, two solar panels and one white antenna. We consider that the body is entirely covered with MLI, and that only one antenna participated to the maximum light because no more is oriented to France or Europe.

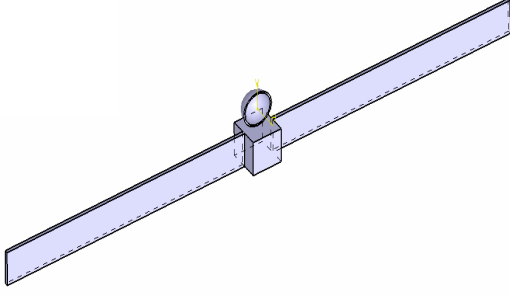


Figure 1. Simplified model of satellite for light curve simulations

The satellite magnitude depends on the conditions of illumination which are bound with the geometrical configuration of the Sun, the Satellite and the observer.

2.2. The Geometric Lighting Conditions

There are two conditions of illumination to be taken into account. The first is the period of eclipses of satellites in the shadow and the penumbra of the Earth. And the second is the phase angle, i.e. the angle between the sun and the observer seen from satellite.

We used the following parameters:

E_0 : Solar constant, $E_0=1400\text{W/m}^2$,

Δ : distance between Earth and surface, $\Delta = 42164$ km for a geostationary satellite,

r : distance between the Sun and surface, $149\,555\,706$ km $< r < 149\,640\,034$ km for a geostationary satellite,

Tr : area of the small surface,

ρ_A : diffusion albedo of the small surface,

k_S : specular coefficient of the small surface,

\mathbf{n} : normal vector of the small surface steered towards the centre of gravity of the satellite,

α : phase angle,

θ_S : angle between the vector \mathbf{r} of direction satellite-Sun and the vector \mathbf{n} ,

θ_E : angle between the vector Δ of direction satellite- Earth and the vector \mathbf{n} ,

φ_S : half-diameter of the Sun seen from satellite,

φ_E : half-diameter of the Earth seen from satellite,

R_S : radius of the Sun,

R_E : radius of the Earth,

μ : diffusion coefficient depending on the surface state.

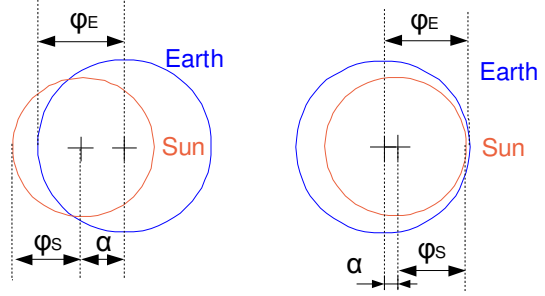


Figure 2. Phase angle and half-diameter seen from satellite around equinox that shows the penumbra on the left panel and the shadow on the right [8]

We can define φ_S , φ_E and α by Eqs. 1-3:

$$\varphi_S = \arcsin\left(\frac{R_S}{r}\right) \quad (1)$$

$$\varphi_E = \arcsin\left(\frac{R_E}{\Delta + R_E}\right) \quad (2)$$

$$\cos(\alpha) = \frac{\vec{\Delta} \cdot \vec{r}}{\Delta r} \quad (3)$$

From Fig. 2 we can verify that the observed object will be in the shadow of the Earth in the conditions of the Eqs. (4).

$$\alpha < \varphi_E - \varphi_S \text{ and } \varphi_E > \varphi_S \quad (4)$$

The observed object will be in the penumbra of the Earth when:

$$|\varphi_E - \varphi_S| < \alpha < \varphi_E + \varphi_S \quad (5)$$

The rest of the time, the satellite is lighted up by the Sun and is visible from the Earth all the nights.

2.3. The Satellite Illumination

We approximate here the Sun as an isotropic black body source. The diffused illumination by a small surface of a satellite, received at the level of the Earth is given by Eq.(6) in $[\text{W/m}^2]$.

$$E_T = \frac{E_o}{16\pi^2 \Delta^2 r^2} \times Tr \times \rho_A \times \cos(\theta_S) \times \cos(\theta_E) \times \mu \quad (6)$$

If the surface is smooth and homogeneous, the reflection of sunbeams will be specular: the light will be reflected in a symmetric direction about the incidental ray with regard to the normal.

In most of the cases, the natural surfaces provoke diffuse reflections, distributed in several directions. If,

the diffused energy is exactly the same in all the directions, the surface is said Lambertian. In this case the diffusion coefficient is: $\mu=1$.

Other models are closer to the reality. The distribution of Lommel-Seelinger realizes compromise between an ideal Lambertian diffuser and a real surface [9]. This law, at first proposed by Lommel then modified by Seelinger was one of the first ones proposed for the photometry of the natural satellites, the porous or rocky asteroids and the planets. The diffusion coefficient is given by Eq.7.

$$\mu = \frac{1}{\cos(\theta_S) + \cos(\theta_E)} \quad (7)$$

The model can be improved for surfaces considered as bright (e.g. antennae). Phong introduces a term of specular reflection on top of the Lambertian in the case of a very bright source (Eq.8-9) [10], [11].

$$\mu = 1 + k'_s \times \cos^m(\theta_S - \theta_E) \quad (8)$$

$$k'_s = \frac{k_s \times 16\pi^2 \Delta^2 r^2}{Tr \times \rho_A \times \cos(\theta_S) \times \cos(\theta_E)} \quad (9)$$

Where m is a mesure of relative intensity into the cone of reflection and k_s the specular coefficient of the material.

We simulated the lighting received from the surfaces of a geostationary satellite with these three distribution laws.

3. THE SIMULATIONS OF SATELLITE MAGNITUDE

The surface of each satellite part has been modeled using a triangular mesh. The coordinates of each point are defined in the equatorial satellite frame and save into a STL format file [12].

The simulation is based on the ellipsoid model for minor planet [13] implemented on the free astronomical software AudeLa (<http://www.audela.org/>).

The total illumination received on the telescope is the sum of each triangle illumination. The visual magnitude m is computed for all the illumination laws with the Pogson relation (Eq. 10).

$$m = -2.5 \times \log(E) + d \quad (10)$$

E is the total flux received by the telescope. d is the instrumental constant determined for each image by

differential photometry with the USNO-B2 astronomical catalogue [14], [15].

Table 2: parameters used for light curves simulations

Satellite part	Material	Solar reflection for new material	Diffuse albedo ρ_A	Reflection law
Body	MLI	0.67	0.1	Lommel-Seelinger
Solar spans		0.15	0.02	Lommel-Seelinger
Antennas/ Equivalent surface	White paint	0.8	0.2	Phong

For each satellites of Tab.1, we add the light curves obtained for each satellite parts with the parameters describe on the Tab.2.

Fig. 3 displays the simulation obtained for Syracuse 3A on the night of March 1st, 2008.

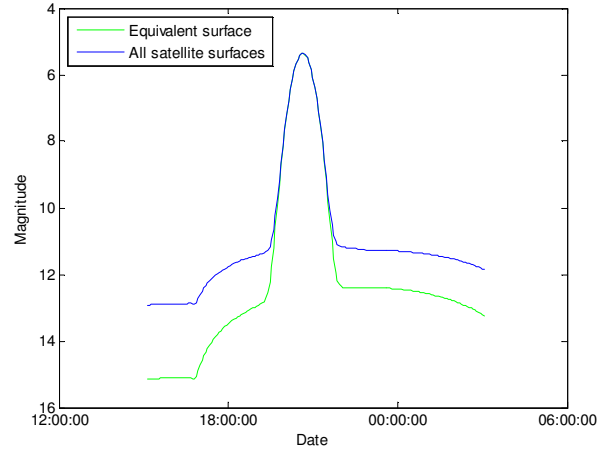


Figure 3. Light curves of Syracuse 3A - Night of March 1st, 2008

The Phong reflection law needs parameters. We choose to assign to the equivalent surface of the antennas the brightness constant $m=150$ (smooth surface) and $k_s = 500$. The umbra and penumbra phase are not represented on the figure 3.

4. TAROT OBSERVATION

In October 2007 and March 2008 we observed a light flare for some GEO satellites with TAROT Calern. For specular reflection, the maximum of illumination is when the Sun is seen near the geostationary belt. For TAROT Calern it corresponds to -6.8 in declination, corresponding to reached nights of March 1st and October 10th.

We have simulated here light curve for these particular dates (Fig. 4 to Fig. 7). The simulation doesn't take into account the entry into the Earth penumbra. This explains differences between simulations and observations during eclipses.

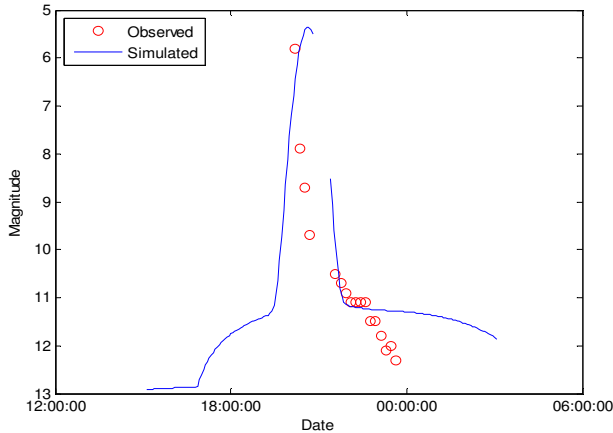


Figure 4. Light curve of Syracuse 3A - Night of the March 1st 2008

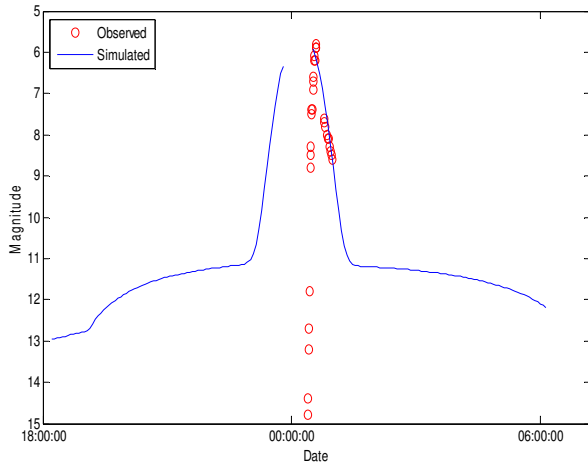


Figure 5. Light curve of Syracuse 3B - Night of the October 11th 2007

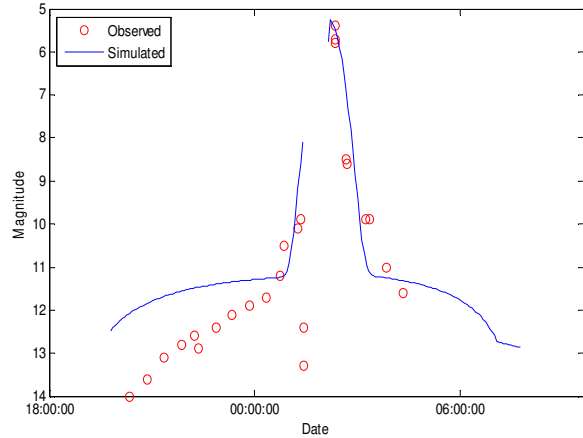


Figure 6. Light curve of Hispasat 1C - Night of the October 10th 2007

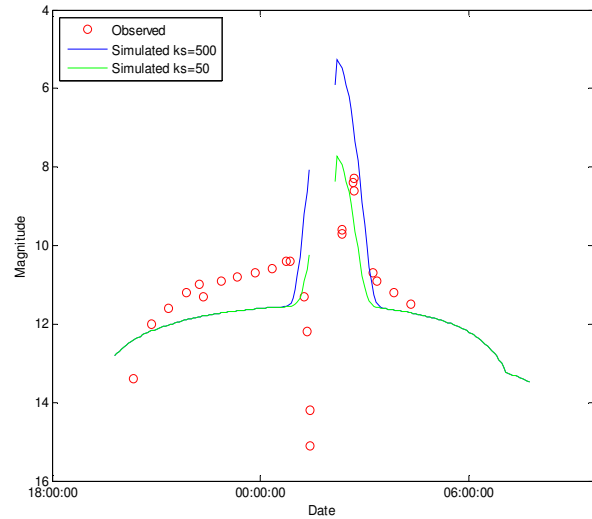


Figure 7. Light curve of Spainsat - Night of the October 10th 2007

The Fig. 7 gives the simulations for two different values of k_s . From Eqs. 6, 8-9 dividing k_s is equivalent to reduce the surface into simulations. According to simulations, the equivalent surface of Spainsat is two time smaller than that Hispasat 1C, Syracuse 3A or Syracuse 3B. We see that Spainsat antennas are smaller than other observed satellites (www.arianespace.com and http://space.skyrocket.de/index_frame.htm?http://www.skyrocket.de/space/doc_sat/).

We conclude that when we exclude the penumbra, simulations are quite good. We can predict for all geostationary objects the illumination peak due to the specular reflection of some surfaces.

5. DISCUSSION AND CONCLUSION

This phenomenon opens new debris detection strategy. Since we know in which conditions the flare occurs, we can take images during the night of the area in order to detect smaller objects. Furthermore, we can deduce from the flare intensity surface information: size or geometric albedo. This can be used in two ways: first, we can enhance the sensitivity of surveys and detect smaller objects. Second, we can characterize unknown objects (equivalent surface size, albedo, reflection law ...). If we have the appropriate information on a satellite and adequate model, it is also possible to get information on its attitude.

We presented simulations of object brightness based on two reflection law. This phenomenon is essentially seasonal (March and October in Europe). The model is validated by TAROT observations.

6. REFERENCES

1. Jehn, R., Agapov, V., and Hernández, C. (2005). The situation in the geostationary ring. *Adv. Sp. Res.*, 35, 1318-1327.
2. Klotz, A., Boër, M., Eysseric, J., Damerdji, Y., Bourez-Laas, M., Pollas, C., and Vachier, F. (2008). Status of the robotic TAROT observatories: Period 2004-2007. *PASP*, 120, 1298-1306.
3. Boër, M., Atteia, J. L., Damerdji, Y., Gendre, B., Klotz, A., Stratta, G. (2006). Detection of a Very Bright Optical Flare from the Gamma-Ray Burst GRB 050904 at Redshift 6.29. *Astron. J.*, 638, L71-L74.
4. Klotz, A., Boër, M., Atteia, J. L., Gendre, B. (2009). Early optical observations of GRB sources by the TAROT telescopes: period 2001-2008. *Astron. J.*, in press.
5. Klotz, A., Vachier, F., and Boër, M. (2004). TAROT: Robotic observatories for gamma-ray bursts and other sources. *Astro. N.*, 329, 275.
6. Deguine, B., Thiebaut, C., and Alby, F. (2004). Optical Observations of Space Debris and Satellites, *AIAA "Space Operations Communicator"*. july/september issue 2004.
7. Meyer, R. X. (1990). *Elements of space technology for aerospace engineers*, Academic press.
8. Kelso, T. S. (1996). Visually Observing Earth Satellites, *Satellites Times*, 3, no.1, 80-82, September/October issue 1996.
9. Horn, B. K. P. (1981). Hill Shading and the Reflectance Map. *Proc. of the IEEE*, 69, 14-47.
10. Ris, P. (1996). *Parallélisation du lancer de rayon par évaluation dynamique de la topologie de la scène*, Thèse de doctorat septembre 1996.
11. Phong, B. T. (1975). Illumination for Computer Generated Pictures, *Communications of the ACM*, 18, 311-317, June 1975.
12. Rypl, D., and Bittnar, Z. (2006). Generation of computational surface meshes of STL models. *Journal of Computational and Applied Mathematic*, 192, 148-151, 2006.
13. Klotz, A., Behrend, R., Colas, F., Agneska, A., and Chatilla, Z. (2009). Pole determination for nine binary minor planets, *A&A*, unpublished.
14. Monet, D. G., Levine, S. E., Canzian, B., Ables, H. D., Bird, A. R. and 24 coauthors. (2003). The USNO-B Catalog. *Astron. J.*, 125, 984-993.
15. Bourez-Laas, M., Blanchet, G., Boër, M., Ducrotté, E., and Klotz, A. (2009). New Algorithms for Optical Observations of Space Debris with the TAROT Telescopes. *Adv. Sp. Res.*, in press.